Hindawi
Advances in Materials Science and Engineering
Volume 2022, Article ID 4874834, 10 pages
https://doi.org/10.1155/2022/4874834

Research Article

Potentiodynamic Corrosion Behavior and Microstructural Characteristics of Pulsed CMT-Welded AA2014-T6 Aluminium Alloy Joints: Effect of PWHT

A. Padma Rao,[1] **Manzoor Hadi**,[1] **C. Rajendran**,[2] **Sonar Tushar**,[3] **Mikhail Ivanov**,[3] **P. Senthil Kumar**,[1] **and V. Murali Krishna**[1]

[1]*Department of Mechanical Engineering, Padmasri Dr. BV Raju Institute of Technology, Narasapur 502313, Telangana, India*
[2]*Department of Mechanical Engineering, Sri Krishna College of Engineering and Technology, Coimbatore 641008, Tamil Nadu, India*
[3]*Department of Welding Engineering, Institution of Engineering and Technology, South Ural State University, Chelyabinsk 454080, Russia*

Correspondence should be addressed to Sonar Tushar; tushar.sonar77@gmail.com

Received 22 July 2022; Revised 10 September 2022; Accepted 26 September 2022; Published 10 October 2022

Academic Editor: Michele Fedel

Copyright © 2022 A. Padma Rao et al. This is an open access article distributed under the Creative Commons Attribution License, which permits unrestricted use, distribution, and reproduction in any medium, provided the original work is properly cited.

AA2014-T6 is an Al-Cu-Mg-based precipitation-hardened aluminium alloy widely used in aerospace due to its high strength to weight ratio. This alloy is joined by a pulsed cold metal transfer (PCMT) arc welding process to overcome the high heat input related problems in gas metal arc welding (GMAW) such as a coarser dendritic structure in the fusion zone (FZ), wider heat affected zone (HAZ), solidification and HAZ liquation cracking, softening in HAZ, and poor corrosion resistance of welded joints in salt environment. The joints were subjected to PWHT of artificial aging (AA), solution treatment (ST), and solution treatment + aging (STA) conditions. The corrosion rate was determined using a potentiodynamic corrosion test in a solution of 3.56 wt.% NaCl with pH values of 4, 7, and 11. Results disclosed that the PCMT joints subjected to the potentiodynamic corrosion test in NaCl solution of pH-4, pH-7, and pH-11 disclosed very low, moderate, and extremely high pitting corrosion, respectively. The corrosion resistance of ST joints was improved by 53.34%, 15%, and 15.12% in pH-4, pH-7, and pH-11 NaCl solution compared to as-welded joints. The pitting potential of ST joints is comparable to BM. The BM showed the pitting potential of −175, −450, and −550 mV in pH-4, pH-7, and pH-11 NaCl solution. The ST joints showed 75.29%, 29.16%, and 27.85% lower corrosion potential compared to STA joints in pH-4, pH-7, and pH-11 NaCl solution, respectively. The ST joints disclosed the lower pitting potential of −105, −425, and −505 mV in pH-4, pH-7, and pH-11 NaCl solution, respectively, whereas the STA joints revealed greater pitting potential of −425, −600, and −700 mV in pH-4, pH-7, and pH-11 NaCl solution, respectively. The superior corrosion resistance of ST joints compared to AA and STA joints is attributed to the dissolution of precipitates in Al solid solution resulting in a lower potential difference in FZ. This minimizes the preferential sites for pitting corrosion to occur.

1. Introduction

AA2014-T6 is high strength heat-treatable Al alloy extensively employed in defense and aerospace sectors owing to its superior higher strength/weight ratio, good characteristics of formability, and corrosion resistance [1]. The joining of this alloy by fusion welding is very much challenging owing to the appearance of a harder oxide layer of aluminium (Al_2O_3), excellent thermal conductivity and thermal expansion coefficient, shrinkage during solidification, and entrapped gases in FZ [2]. This alloy is mainly welded by a gas metal arc welding (GMAW) process. However, the high heat input and lower arc penetration in GMAW leads to the evolution of a detrimental coarser dendritic structure in the fusion zone (FZ), wider heat affected zone (HAZ), solidification and HAZ liquation cracking, and softening in HAZ [3]. This significantly deteriorates the strength performance and corrosion resistance of welded joints particularly in the salt environment. Also,

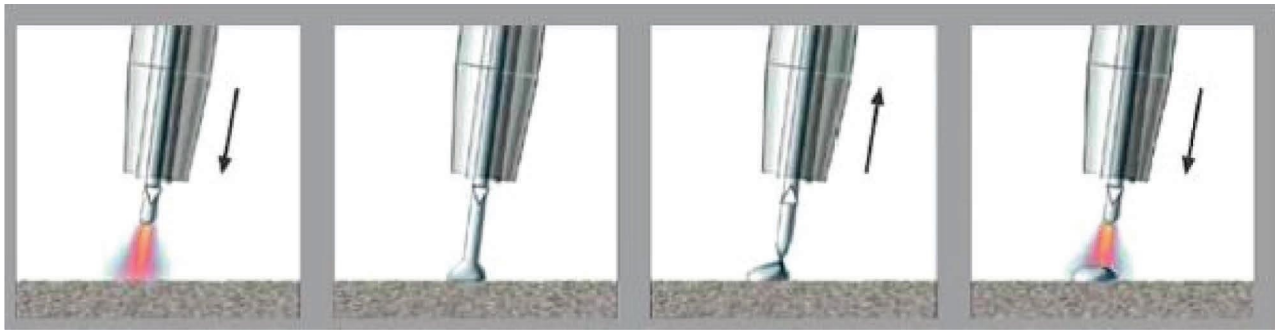

Figure 1: Working principle of CMT welding [4].

joining thin sheets of AA2014-T6 alloy by GMAW is challenging owing to greater residual stresses and distortion related problems. To overcome these problems, a pulsed cold metal transfer (PCMT) arc welding process mainly featured by filler wire feeding and retraction mechanisms was employed to join 2 mm thick sheets of the AA2014-T6 aluminium alloy, which significantly lowers the heat input-related problems in GMAW of 2014-T6 alloy. In CMT-welding, short circuit timing is detected by the digital control and the droplets are detached by retraction of a filler wire. The wire is pushed forward and is reverted back on short circuiting. It is based on short-circuit mode of weld metal transfer invented by Fronius Austria. In CMT, as the tip of filler wire contacts the molten puddle, the digital process control reverses the servomotor of CMT torch which causes the retraction of the filler wire and ensues metal transfer in droplet mode as shown in Figure 1 [4]. The waveform of CTM welding arc is shown in Figure 2. The generation of spatter in CMT-welding is avoided as the welding current falls down to zero value during transfer of metal. The CMT arc is regenerated as soon as the mode of transfer of metal is finished and the filler wire is moved forward with the pre-set welding current. CMT welding offers the advantages of increased deposition rate, lower heat input, spatter, and dilution over GMAW [5].

Çömez and Durmuş [6] investigated the corrosion performance of CMT-welded AA6061-AA7075 Al alloys and reported that the corrosion rate of joints increases from 0.16 mm/year to 1.3 mm/year at increased levels of heat input from 77.1 J/mm to 128.4 J/mm. Elrefaey [7] investigated the joint characteristics of CMT-welded AA7075-T6 Al alloys and reported that the CMT joints exhibited 77%, 60% and 69% of yield strength, tensile strength, and elongation of the base metal, respectively. Huan et al. [8] evaluated the strength performance of CMT-welded 6063 Al alloy made using ER4047 and ER5183 filler wires and reported that the strength of ER5183 joints (85.7%) was greater than ER4047 joints (68.1%). Ramaswamy et al. [9] evaluated the joint characteristics of PCMT-welded and GMA-welded 6061-T6 alloys and observed that PCMTW joints exhibit 16% improvement in strength compared to GMAW joints. Çömez and Durmuş [10] investigated the corrosion performance of CMT-welded dissimilar AA5754-AA6061 alloys and reported that the corrosion rate of joints increases from 0.053 mm/year to 0.24 mm/year at increased heat input levels from 71.25 J/mm to 112.75 J/mm. Madhavan et al. [11]

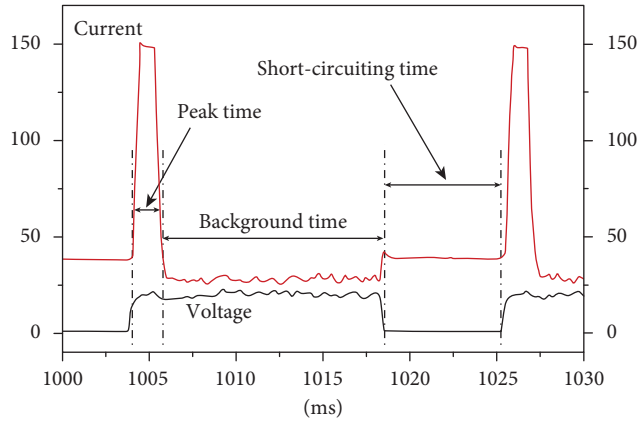

Figure 2: Waveform of current and voltage in CMT welding [4].

analyzed the corrosion performance of CMT-welded dissimilar AA6061-AZ31B alloys and reported that the joints developed using 205 J/mm heat input disclosed a superior tensile strength of 360 MPa and greater resistance to pitting corrosion. Ramaswamy et al. [12] analyzed the influence of PWHT on strength performance of CMT-welded AA6061-T6 joints and reported 10% improvement compared to as-welded joints owing to the improved precipitation in FZ. Ahmad and Bakar [13] studied the PWHT effect on mechanical performance of CMT-welded AA6061-T6 joints and reported 3.8, 25.6, and 21.5% enhancement in strength, hardness, and ductility of joints owing to the refinement and uniform precipitation in the FZ.

The literature review confirmed that the research work reported on CMT-welding of AA2014-T6 alloy joints, so far, is limited. There is lack of investigation on corrosion performance of CMT-welded AA-2014-T6 alloy joints in corrosive salt environment. This necessitates the study on influence of PWHT and potentiodynamic corrosion performance of AA2014-T6 joints in different conditions of salt water environment. Hence, the main objective of this investigation is to assess the influence of postweld heat treating (PWHT) conditions on potentiodynamic corrosion performance of PCMT-welded AA2014-T6 alloy joints.

2. Experimental Work

The AA2014-T6 alloy (2 mm thick) and ER4043 wire of diameter 1.2 mm was chosen as a base material (BM) and a

Table 1: Chemical composition (wt-%) of the AA2014-T6 aluminum alloy and ER4043 filler wire.

Material	Si	Fe	Cu	Mg	Cr	Zn	Ti	Mn	Al
AA2014-T6	0.86	0.11	4.72	0.72	0.004	0.05	0.01	0.801	Bal
ER4043	5.6	0.8	0.3	0.05	0.05	0.1	0.02	0.05	Bal

Table 2: Mechanical properties of the AA2014-T6 aluminum alloy and ER4043 filler wire.

Material	0.2% yield strength (MPa)	Tensile strength (MPa)	% Elongation (50 mm gauge length)	Microhardness (HV)
AA2014-T6	429	452	8.3	159
ER4043	164	190	--	--

Table 3: Postweld heat treatment cycles used in this investigation.

Sr. No.	PWHT	Cycle
1.	Solutionizing (ST)	Solutionizing at 500°C for 1 hour
2.	Solutionizing + artificial aging (STA)	Solutionizing at 500°C for 1 hour + artificial aging at 165°C for 10 hours
3.	Artificial aging (AA)	Artificial aging at 165°C for 10 hours

filler material in this investigation. The chemical composition and mechanical properties of BM and filler wire are reported in Tables 1 and 2. The butt joints were developed employing pulsed cold metal transfer (PCMT) welding using optimized parameters. The postweld heat treatment cycles used in this investigation are presented in Table 3. The photograph of the PCMT welding machine and is shown in Figure 3. The joints were developed in a butt joint design as per the dimensions shown in Figure 4. The photograph of fabricated PCMT joint is shown in Figure 5. The optimized PCMT parameters were used to develop the butt joints as presented in Table 4. The process parameters were selected by observing the defects such as porosity, incomplete penetration, excess penetration, and undercuts in welding trials. The specimens were cut in 20×30 mm sizes for the potentiodynamic corrosion test. The specimens were polished to 1 μm surface finish using emery papers and diamond polishing. The specimens were etched by a prepared reagent. The microstructure of PCMT weld region was analyzed using optical microscopy. Transmission electron microscopy (TEM) was employed to analyze the precipitation influenced by PWHT.

The corrosion performance of joints was analyzed employing a potentiodynamic polarization test. It was done in 3.56 wt.% NaCl solution at different levels of pH (4—acidic, 7—neutral, and 11—basic). The etched specimens were subjected to a corrosion test for the FZ. The test setup contains an electrochemical cell with a reference electrode (saturated calomel electrode), a working electrode (weld sample), and a counterelectrode (graphite electrode). The test was done as per the ASTM standard of G59 at 28°C employing Gill AC potentiostat (Make: ACM Engineering & Model: Gill AC 951) at a scanning rate of 1 mV/sec in the span of −250 mV to 250 mV. By polarizing the specimen anodically and catholically, the Tafel plots were plotted. The current density in corrosion and i_{corr} values were determined by intersection of these two lines at corrosion potential. For each Tafel plot, current density and potential in corrosion were observed directly from the polarization setup.

3. Results and Discussion

The optical micrograph of BM in as-received condition is presented in Figure 6. It exhibits coarse and elongated grains aligned along the rolling direction. The average size of grains is 30 μm. The optical micrographs of joints under different conditions of PWHT are shown in Figure 7. In PCMT weld, the joint is formed by a heterogeneous microstructure due to differences in peak temperature and cooling rate at various zones. The FZ showed equiaxed dendritic grains due to low heat input and rapid solidification. The coarse grain structure was observed in HAZ. PWHT extends significant influence on the microstructure of FZ and HAZ of AA2014-T6 joints. The as-welded joints showed a comparatively coarser dendritic FZ microstructure. When the joints were subjected to PWHT of ST, STA, and AA, there is refinement in the dendritic FZ microstructure. The grain growth was also observed to be reduced in HAZ of joints when subjected to ST, STA, and AA. The ST joints exhibited a much finer dendritic FZ microstructure compared to STA and AA joints. Also, the grain size in HAZ of ST joints is minimized compared to STA and AA joints. The TEM micrographs of base metal and FZ of as-welded joints, ST, AA, and STA joints are presented in Figure 8. It shows the presence of strengthening precipitates in base metal and FZ of joints. The precipitation in ST joints is much lower compared to other joints as the solution annealing results in dissolution of precipitates in the Al matrix. The AA and STA joints exhibit more precipitation compared to other joints. The precipitates in AA joints are needle-shaped, whereas they are spherical in STA joints. The EDS analysis of base metal, FZ of as-welded joints, ST, AA, and STA joints is shown in Figure 9.

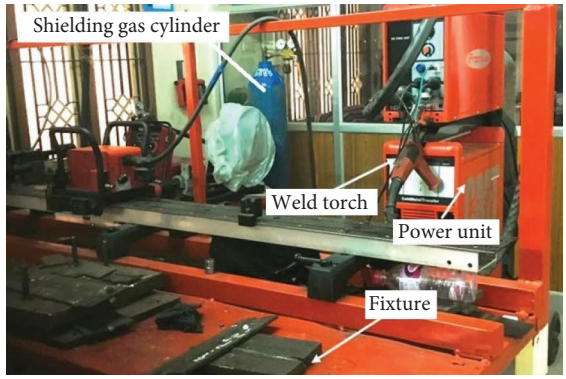

Figure 3: Photograph of CMT-welding machine setup.

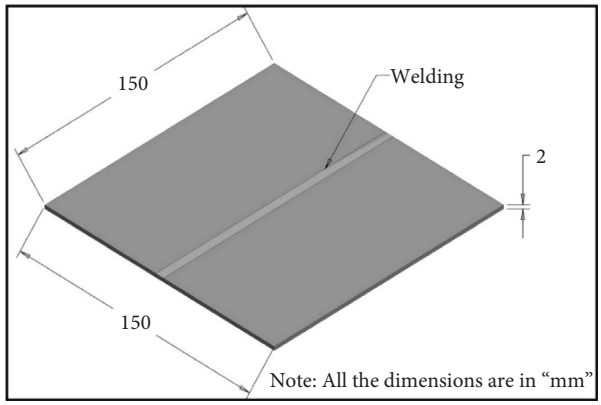

Figure 4: Butt joint configuration used to develop the joints.

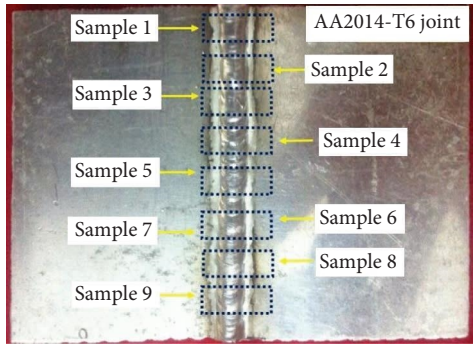

Figure 5: Photograph of the joint.

The elemental% of Al and Cu is more in AA and STA joints due to the increased precipitation. The precipitation offers preferential sites for pitting corrosion to occur in joints due to chemical heterogeneity and more potential difference between the Al matrix and precipitates in FZ. The second phase precipitation gives rise to potential difference between FZ and BM and thereby offers poor resistance to pitting corrosion [14]. It is evidenced by the optical micrographs of corrode specimens as displayed in Figure 10showing greater pitting corrosion in AA joints. The ST joints revealed less pitting corrosion compared to

Table 4: PCMT welding parameters used in this investigation.

Sr. No	Parameters	Values
1	Arc voltage	10 V
2.	Welding current	100 a
3.	Rate of wire feed	5400 mm/min
4.	Welding speed	425 mm/min
5.	Arc length	12
6	Heat input	0.213 kJ/mm

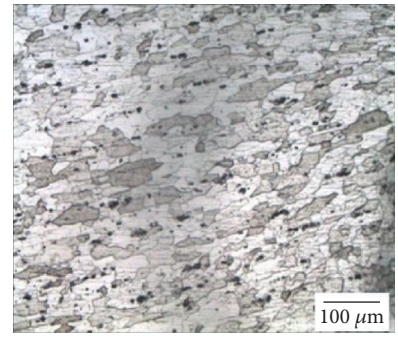

Figure 6: Optical micrograph of the as-received AA2014-T6 alloy.

AA and STA joints. Generally, the corrosion resistance of metal increases with increases in grain size. The coarser grain microstructure is generally less susceptible to corrosion than the finer grain microstructure due to the less grain boundary energy. This effect can be seen in base metal. However, the inverse relationship was observed between grain size and corrosion resistance of welded joints. It is mainly due to the difference in microstructural characteristics and precipitation behavior in different regions of welded joints such as FZ, HAZ, and BM. The coarser dendritic FZ microstructure is more susceptible to corrosion than a finer dendritic FZ microstructure due to the less alloying segregation in interdendritic region and uniform distribution of second phase precipitates. The ST joints showed greater refinement in the dendritic FZ microstructure. The dendritic FZ microstructure of STA and AA joints is coarser compared to ST joints and exhibit nonuniform second phase precipitation. The second phase precipitation in STA joints is coarser in the form of needles, whereas the second phase precipitation in AA joints is finer. This is the main reason the STA joints showed a greater corrosion potential compared to AA joints. The ST joints exhibit less chemical heterogeneity due to the refinement in dendritic FZ microstructure and absence of second phase precipitation. Thus, the finer dendritic FZ microstructure and absence of second phase precipitation in FZ are the main reasons for greater corrosion resistance of SZ joints compared to STA and AA joints.

Polarization curves of PWHT joints of AA2014 alloy are shown inFigures 11–13. The potential value in pitting corrosion (E_{pit}) was considered as the important factor for pitting corrosion resistance comparison. E_{pit} for various types of welds were computed experimentally, and the results are presented in Table 5. If the potential value (less -ve and more + ve) offers high corrosion resistance. From the

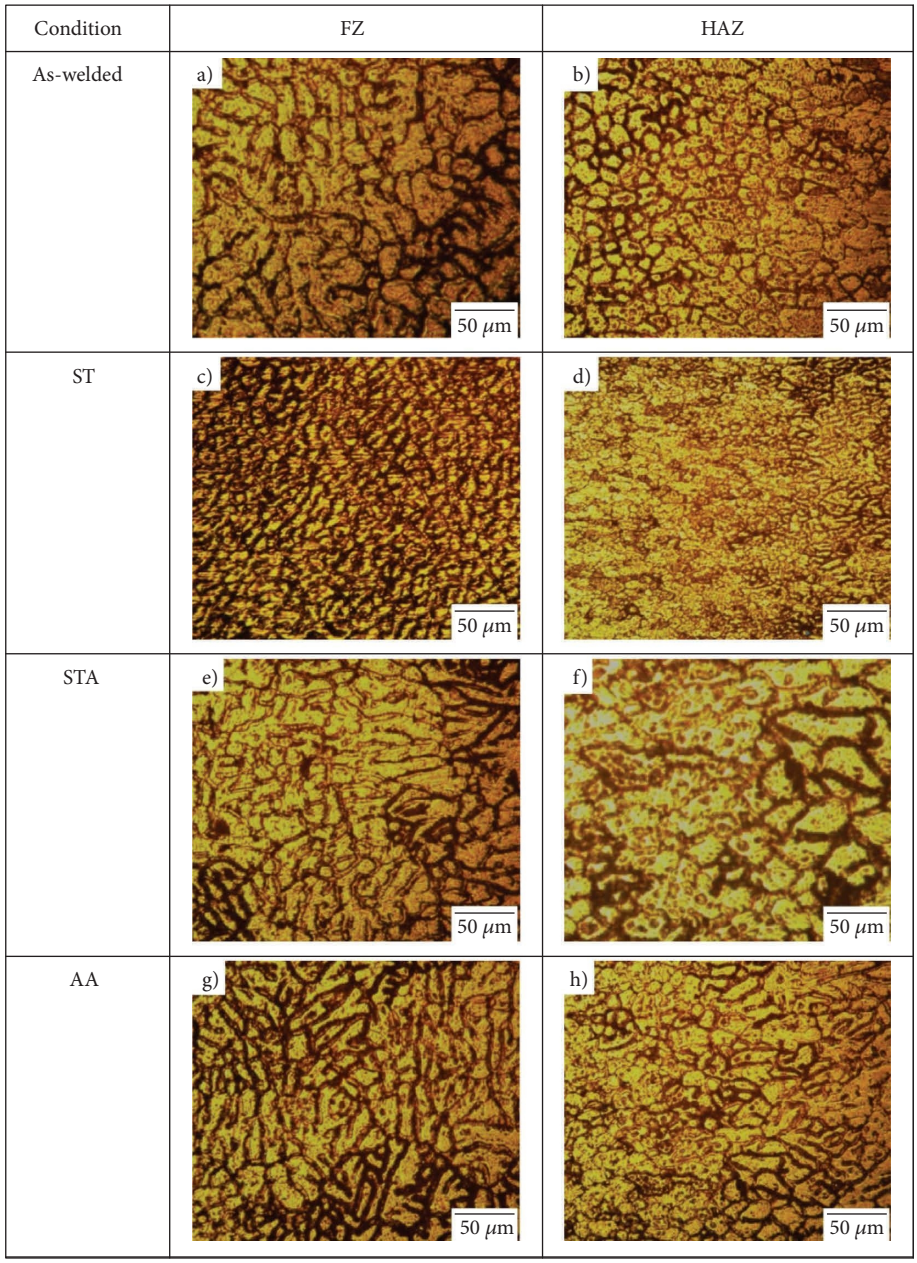

Figure 7: Optical micrographs of joints of AA2014-T6 alloy: (a), (c), (e), and (d) FZ of as-welded, ST, STA, and AA joints; (b), (d), (f), and (h) HAZ of as-welded, ST, STA, and AA joints.

experimental results, it is found that ST joints offer greater corrosion resistance than its counterpart, also superior corrosion resistance (pitting potential) than the BM. Except for ST, all other joints were shown to be deleterious to resistance in corrosion of the welds. Although, low pitting corrosion was observed in pH 4 solution. On the other hand, high corrosion was observed in pH 11 solution and medium corrosion was noticed in pH 7 solution. Pitting corrosion in Cu-containing aluminum alloy is a function of exposure time and environmental conditions. Pitting corrosion is introduced by precipitates/intermetallic compounds such as $CuAl_2$ and Al_6 (CuFeMn).

The base metal region exhibits coarser elongated grains. The grain structure changes to a dendritic structure in FZ after fusion welding. The corroded joints showed the evolution of pits on the dendrite boundaries. The dendritic structure is more susceptible to corrosion than the base metal grain structure. It is attributed to the alloying segregation that occurs during fusion and heterogeneous distribution of second phase precipitation in FZ. The variation in grain size and structure in FZ and HAZ of joints also increases the corrosion potential. The formation of intermetallic is formed by combination of two or more alloying elements in matrix during the heating and cooling cycle. In the Al-Cu binary phase system, the most expected intermetallic are Al_7Cu_2Fe, $(Al, Cu)_6(Fe, Cu)$. However, $CuAl_2$ precipitates undergo phase transition and modify their shape during the welding cycle [15]. There is a galvanic

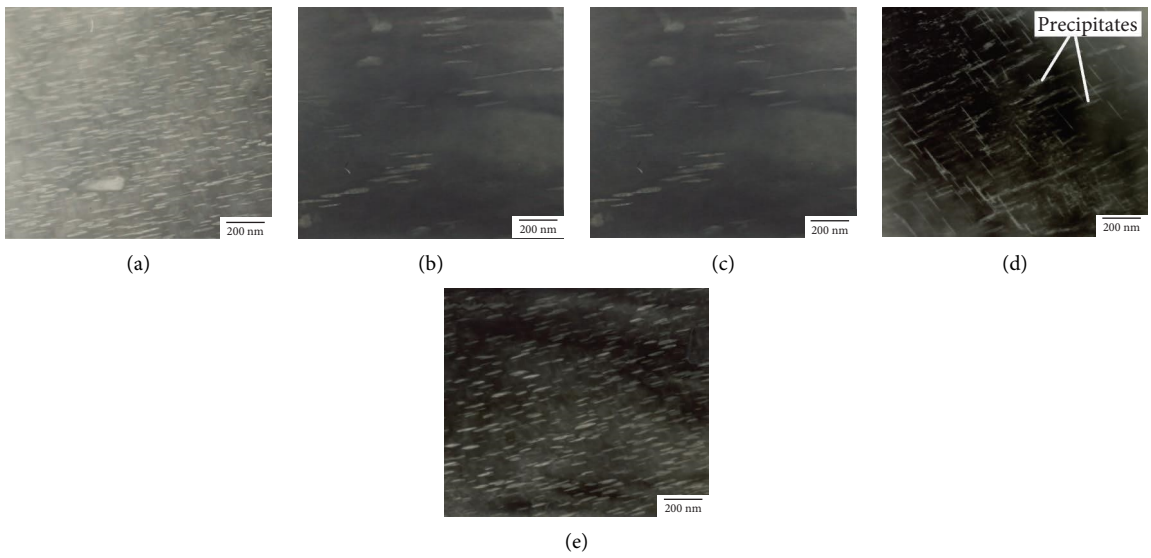

Figure 8: TEM micrographs of base metal and FZ of joints: (a) Base metal; (b) FZ of as-welded joint; (c) FZ of ST joint; (d) FZ of AA joint; and (e) FZ of STA joint.

interaction between intermetallic and matrix. Pitting is caused by local dissolution of the intermetallic or dissolution of the matrix or Fe- and Cu-containing intermetallic negative charge to the matrix and enhances matrix dissolution. Whereas, Cu-based intermetallic charges are positive to the matrix and dissolve favorably. The reinforcing particles in PCMT welds have a $CuAl_2$ composition and are nanometer in size. The alloy's strength is provided by their second phase particle in the Al matrix after age. The pitting corrosion resistance is purely dependent on the formation of second phase particles [16]. Due to less volume of precipitates dissolution during welding, a lesser number of strengthening particles are accessible in AW joints, reducing the count of possible preferred initiation sites for pitting corrosion. This could explain why this joint is more resistant to pitting corrosion than STA and AA joints. ST completely dissolved second phase particles in solid solution. Hence, the count of possible enucleation sites for pitting corrosion in this joint was greatly reduced. This could be a main reason for AA joints possessing superior corrosion resistance when compared to its counterpart. Owing to AA, the appearance of precipitates is inevitable in AA joints, and a large number of precipitates were formed compared to AW, AA, and STA joints, ensuing in additional satisfactory nucleation sites for pitting corrosion [17]. This might be owing to the reduced corrosion resistance of these joints compared to ST and AA joints.

Finer size and density distribution of precipitates were observed in STA joints. This could be achieved by the combined process of ST followed by AA. Hence, a significant number of starting sites are accessible for pitting corrosion, which might be explained why the STA joint has poor resistance in pitting corrosion. The heat of welding may reduce the corrosion resistance of some heat-treatable alloys, particularly those containing significant concentrations of Cu and Zn. Grain boundary precipitation occurs in the HAZ of these alloys, which is frequently anodic to the rest of the weldment. Selective corrosion on grain boundaries can occur in a corrosive environment and this corrosion can accelerate in the presence of stress. Heat treatment after welding gives these alloys a more homogenous microstructure and increases their corrosion resistance. In the AW state, when exposed to a corrosive medium, welds made of Al-Cu alloy were discovered to be attacked preferentially around the weld bead [1]. This preferential attack was avoided by ageing the weld for a long enough period at a high enough temperature. Inadequate aging led in a knife-edge attack parallel to the weld at a distance [18]. The HAZ in Al-Cu alloys becomes cathodic, but in Al/Zn alloys, the rest of the weldment becomes anodic to it. For 2xxx series weldment, the corrosion potentials vary across the weld zone, and these changes in potential can contribute to localized corrosion. Even though the HAZ in the 5xxx aluminum is somewhat cathodic, it is more cathodic in the 2xxx alloy. The HAZ of 7xxx series is anodic to unprocessed material and would be extremely dangerous [19].

It is critical to use the right filler wire to eliminate welding cracks and maximize corrosion resistance. Optimal corrosion resistance is achieved when the filler's solution potential matches that of the BM. In certain situations, the ultimate corrosion resistance of the weld is determined by the intermetallic phase generated by the BM and filler wire. $CuAl_2$ in AA2014 is an intermetallic phase that is detrimental to weldability and corrosion resistance. This intermetallic particle creates liquation in the partly melted zone (PMZ) of the weld seam, resulting in cracking and poor corrosion resistance, as per the chemical interrelationship among those phases with the surrounding matrix. Hu et al. [20] found similar discoveries in the Al-Li alloy welded using

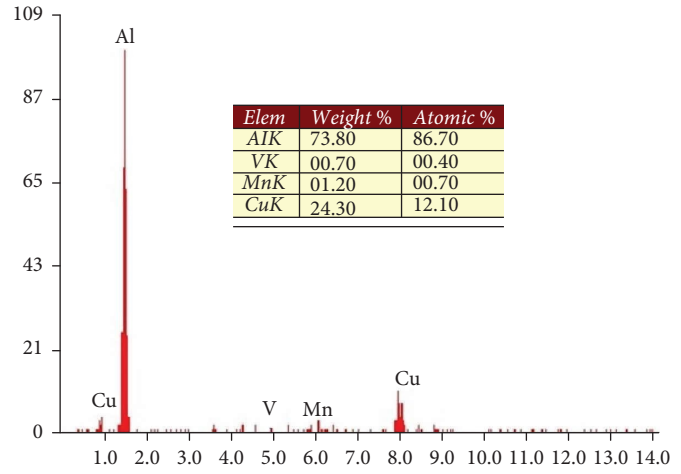

Elem	Weight %	Atomic %
AlK	73.80	86.70
VK	00.70	00.40
MnK	01.20	00.70
CuK	24.30	12.10

(a)

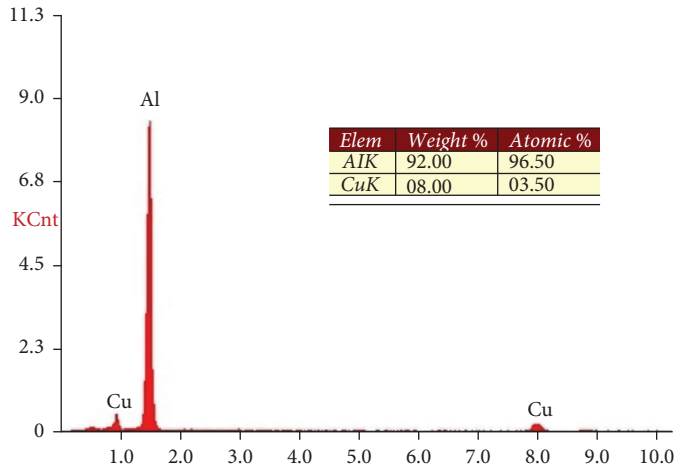

Elem	Weight %	Atomic %
AlK	92.00	96.50
CuK	08.00	03.50

(b)

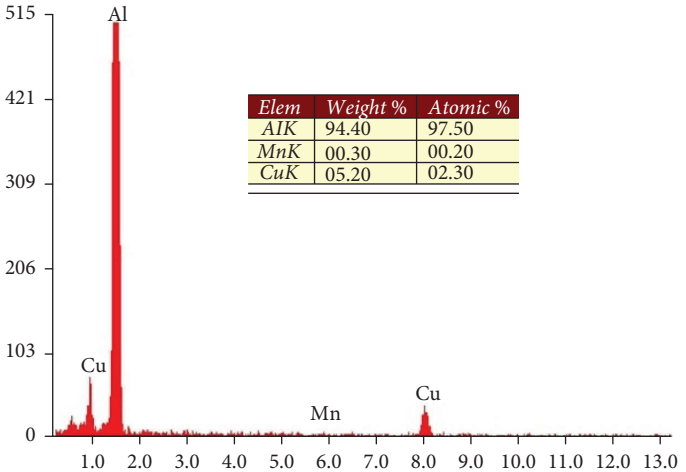

Elem	Weight %	Atomic %
AlK	94.40	97.50
MnK	00.30	00.20
CuK	05.20	02.30

(c)

Figure 9: Continued.

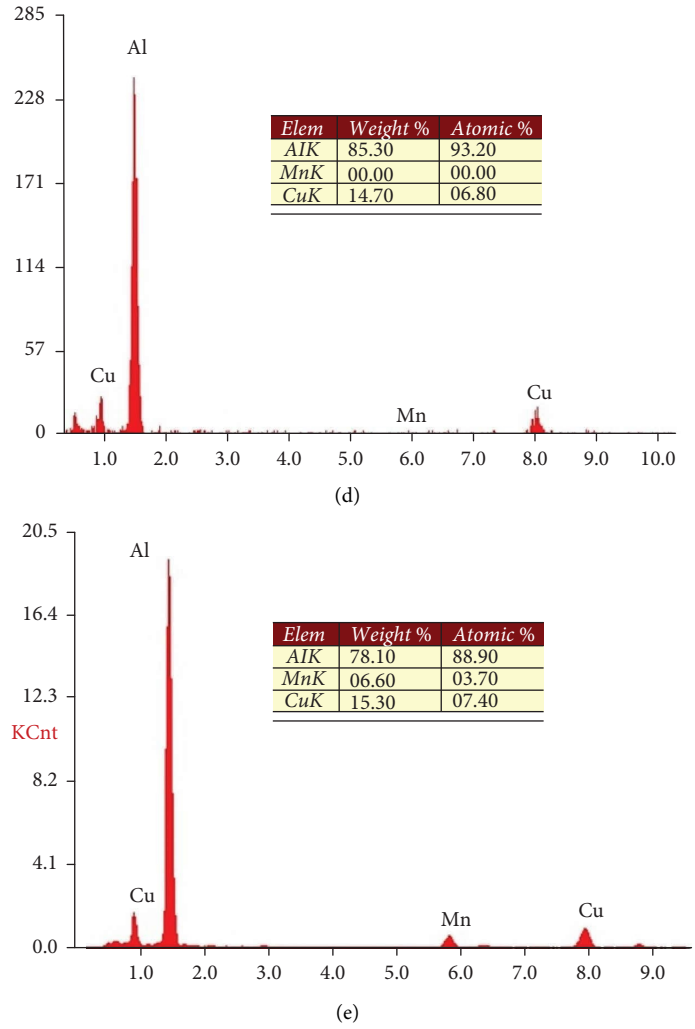

Figure 9: EDS spectrum of FZ of joints: (a) base metal; (b) as-welded; (c) ST; (d) AA; and (e) STA.

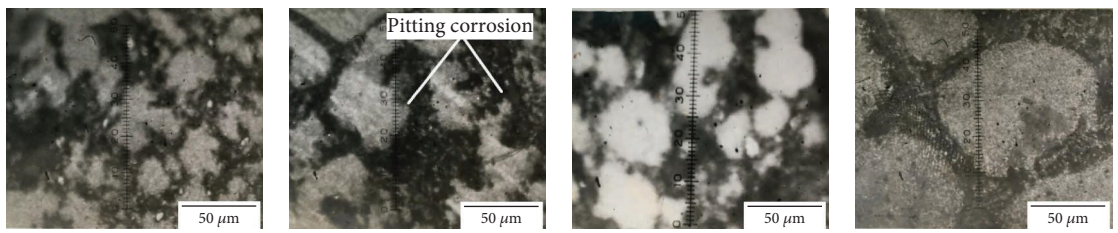

Figure 10: Optical micrograph of corroded joints after PWHT: (a) ST; (b) AA; (c) STA; and (d) BM.

the AA 5356 filler metal. They further claimed that aging to peak strength causes greater equilibrium precipitation at grain boundaries, resulting in a large number of anode-cathode cells. Over aging coarsens the precipitates and causes precipitate agglomeration, resulting in a decrease in precipitate density and the reduction of chemical inhomogeneity surrounding the precipitates owing to diffusional processes [21]. As a result, the overaged condition was a lower susceptibility for corrosion than the underaged and peak aged situations. The alloy in the weldment with the higher negative potential will try to protect the other component. As a result, if the weld metal is anodic to the BM, the tiny weld can be attacked first to preserve the BM greater surface area.

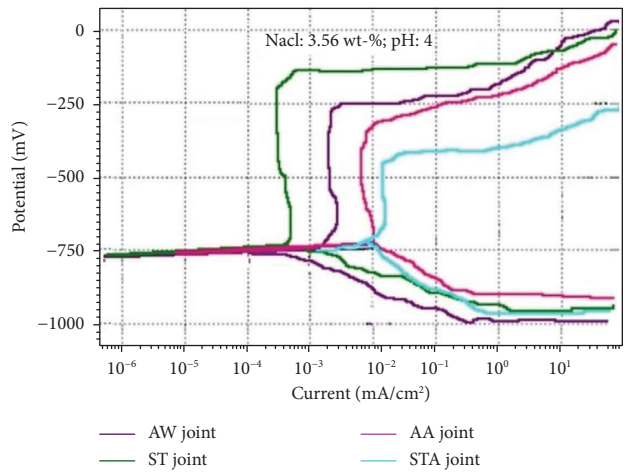

Figure 11: Tafel plot of welded joints in 3.56 wt.% NaCl solution having a pH of 4.

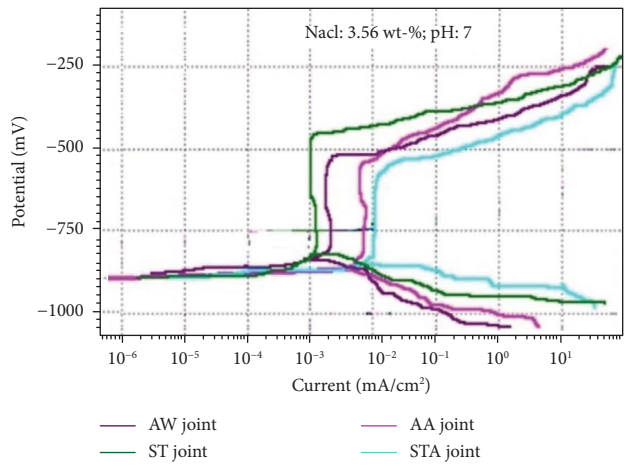

Figure 12: Tafel plot of welded joints in 3.56 wt.% NaCl solution having a pH of 7.

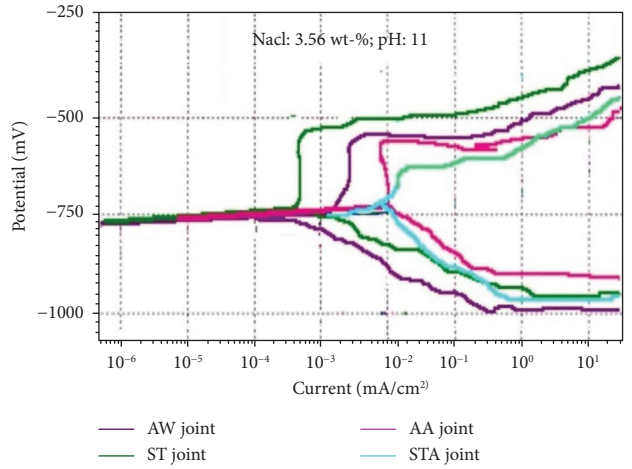

Figure 13: Tafel plot of welded joints in 3.56 wt.% NaCl solution having a pH of 11.

Table 5: Pitting potential values of P-CMT welded AA2014 aluminium alloy joints.

Joint type/Pitting potential (mV)	ST	AA	STA	AW	BM
pH 4	−105	−325	−425	−225	−175
pH 7	−425	−550	−600	−500	−450
pH 11	−505	−650	−700	−595	−550

4. Conclusions

(1) The PWHT showed a significant effect on the microstructure and pitting corrosion performance of PCMT joints of the AA2014-T6 alloy.

(2) The PCMT joints of the AA2014-T6 alloy subjected to a potentiodynamic corrosion test in NaCl solution of pH-4, pH-7, and pH-11 disclosed very low, moderate, and extremely high pitting corrosion.

(3) The PCMT joints subjected to PWHT of ST exhibited superior corrosion resistance than STA and AA joints. The corrosion resistance of ST joints was improved by 53.34%, 15%, and 15.12% in pH-4, pH-7, and pH-11 NaCl solution compared to as-welded joints.

(4) The pitting potential of ST joints is comparable to BM. The BM showed the pitting potential of −175, −450, and −550 mV in pH-4, pH-7, and pH-11 NaCl solution.

(5) The ST joints showed 75.29%, 29.16%, and 27.85% lower corrosion potential compared to STA joints in pH-4, pH-7, and pH-11 NaCl solution, respectively.

(6) The ST joints disclosed the lower pitting potential of −105, −425, and −505 mV in pH-4, pH-7, and pH-11 NaCl solution, whereas the STA joints revealed greater pitting potential of −425, −600, and −700 mV in pH-4, pH-7, and pH-11 NaCl solution.

(7) The superior corrosion resistance of ST joints is attributed to the dissolution of precipitates in the Al matrix, resulting in a lower potential difference in FZ. This minimizes the number of preferential sites for pitting corrosion to occur.

(8) The inferior corrosion resistance of AA joints is attributed to the greater precipitation in the FZ, which increases the potential difference in FZ between the Al matrix and precipitates. Thus, it offers preferential sites for pitting corrosion to occur.

Data Availability

The data used to support the findings of this study are included in the article.

Conflicts of Interest

The authors declare that they have no conflicts of interest.

References

[1] C. Rajendran, K. Srinivasan, V. Balasubramanian, H. Balaji, and P. Selvaraj, "Effect of tool tilt angle on strength and microstructural characteristics of friction stir welded lap joints of AA2014-T6 aluminum alloy," *Transactions of*

Nonferrous Metals Society of China, vol. 29, no. 9, pp. 1824–1835, 2019.

[2] C. Rajendran, K. Srinivasan, V. Balasubramanian, H. Balaji, and P. Selvaraj, "Feasibility study of FSW, LBW and TIG joining process to fabricate light combat aircraft structure," *International Journal of Lightweight Materials and Manufacture*, vol. 4, no. 4, pp. 480–490, 2021.

[3] R. Chinnasamy, S. J. S. Chelladurai, and T. Sonar, "Investigation on microstructure and tensile properties of high-strength AA2014 aluminium alloy welds joined by pulsed CMT welding process," *Advances in Materials Science and Engineering*, pp. 1–8, 2021.

[4] J. Feng, H. Zhang, and P. He, "The CMT short-circuiting metal transfer process and its use in thin aluminium sheets welding," *Materials & Design*, vol. 30, no. 5, pp. 1850–1852, 2009.

[5] S. Selvi, A. Vishvaksenan, and E. Rajasekar, "Cold metal transfer (CMT) technology-An overview," *Defence technology*, vol. 14, no. 1, pp. 28–44, 2018.

[6] N. Çömez and H. Durmuş, "Cold metal transfer welding of AA6061 to AA7075: mechanical properties and corrosion," *Journal of Engineering Materials and Technology*, vol. 141, no. 3, Article ID 031002, 2019.

[7] A. Elrefaey, "Effectiveness of cold metal transfer process for welding 7075 aluminium alloys," *Science and Technology of Welding & Joining*, vol. 20, no. 4, pp. 280–285, 2015.

[8] P. C. Huan, X. N. Wang, J. Zhang et al., "Effect of wire composition on microstructure and properties of 6063 aluminium alloy hybrid synchronous pulse CMT welded joints," *Materials Science and Engineering A*, vol. 790, Article ID 139713, 2020.

[9] A. Ramaswamy, S. Malarvizhi, and V. Balasubramanian, "Effect of variants of gas metal arc welding process on tensile properties of AA6061-T6 aluminium alloy joints," *International Journal of Advanced Manufacturing Technology*, vol. 108, no. 9-10, pp. 2967–2983, 2020.

[10] N. Çömez and H. Durmuş, "Mechanical properties and corrosion behavior of aa5754-aa6061 dissimilar aluminum alloys welded by cold metal transfer," *Journal of Materials Engineering and Performance*, vol. 28, no. 6, pp. 3777–3784, 2019.

[11] S. Madhavan, M. Kamaraj, L. Vijayaraghavan, and K. Srinivasa Rao, "Cold metal transfer welding of dissimilar A6061 aluminium alloy-AZ31B magnesium alloy: effect of heat input on microstructure, residual stress and corrosion behavior," *Transactions of the Indian Institute of Metals*, vol. 70, no. 4, pp. 1047–1054, 2017.

[12] A. Ramaswamy, S. Malarvizhi, and V. Balasubramanian, "Influence of post weld heat treatment on tensile properties of cold metal transfer (CMT) arc welded AA6061-T6 aluminium alloy joints," *Journal of the Mechanical Behavior of Materials*, vol. 28, no. 1, pp. 135–145, 2019.

[13] R. Ahmad and M. A. Bakar, "Effect of a post-weld heat treatment on the mechanical and microstructure properties of AA6061 joints welded by the gas metal arc welding cold metal transfer method," *Materials & Design*, vol. 32, no. 10, pp. 5120–5126, 2011.

[14] T. Sonar, V. Balasubramanian, T. Venkateswaran, D. Sivakumar, and S. Konovalov, "Potentiodynamic corrosion behavior and microstructural features of gas tungsten constricted arc (GTCA)-welded superalloy 718 joints," *Materials Testing*, vol. 63, no. 12, pp. 1116–1123, 2021.

[15] H. Durmuş and N. Çömez, "Soğuk metal transfer kaynağı ile birleştirilmiş aa7075-galvanizli çelik çiftinin korozyon direncinin i?ncelenmesi," *Muş Alparslan Üniversitesi Fen Bilimleri Dergisi*, vol. 7, no. 1, pp. 639–644, 2019.

[16] B. Arulmurugan and M. Manikandan, "Development of welding technology for improving the metallurgical and mechanical properties of 21st century nickel based superalloy 686," *Materials Science and Engineering A*, vol. 691, pp. 126–140, 2017.

[17] X. Xing, X. Di, and B. Wang, "The effect of post-weld heat treatment temperature on the microstructure of Inconel 625 deposited metal," *Journal of Alloys and Compounds*, vol. 593, pp. 110–116, 2014.

[18] S. Sinhmar and D. K. Dwivedi, "A study on corrosion behavior of friction stir welded and tungsten inert gas welded AA2014 aluminium alloy," *Corrosion Science*, vol. 133, pp. 25–35, 2018.

[19] M. A. García-Rentería, V. H. López-Morelos, J. González-Sánchez, R. García-Hernández, L. Dzib-Pérez, and F. F. Curiel-López, "Effect of electromagnetic interaction during fusion welding of AISI 2205 duplex stainless steel on the corrosion resistance," *Applied Surface Science*, vol. 396, pp. 1187–1200, 2017.

[20] Z. Q. Hu, Y. Zhang, Y. L. Liu, and Z. Y. Zhu, "Corrosion behavior of 8090 Al-Li alloy," *Corrosion*, vol. 49, no. 6, pp. 491–498, 1993.

[21] C. Garcia, F. Martin, P. De Tiedra, Y. Blanco, and M. Lopez, "Pitting corrosion of welded joints of austenitic stainless steels studied by using an electrochemical minicell," *Corrosion Science*, vol. 50, no. 4, pp. 1184–1194, 2008.